Optical Materials xxx (2011) xxx–xxx

Contents lists available at ScienceDirect

Optical Materials

journal homepage: www.elsevier.com/locate/optmat

$SrHfO_3$-based phosphors and scintillators

M. Nikl [a,*], P. Bohacek [a], B. Trunda [a], V. Jary [a], P. Fabeni [b], V. Studnicka [a], R. Kucerkova [a], A. Beitlerova [a]

[a] Institute of Physics AS CR, 16253 Prague, Czech Republic
[b] Institute of Applied Physics "N. Carrara" of CNR, 50019 Sesto Fiorentino, Firenze, Italy

ARTICLE INFO

Article history:
Available online xxxx

Keywords:
$SrHfO_3$
Luminescence
Stoichiometry
Ce^{3+}doping

ABSTRACT

The heavily Ce-doped $SrHfO_3$ (SHO) and the undoped non-stoichiometric SHO sample sets were prepared by solid state reaction in powder form and their luminescence spectra and decay kinetics were measured. Concentration quenching effects and thermally induced ionization of the Ce^{3+} excited states were followed and discussed in the former sample set. In the latter one new emission band at about 334 nm was found in Sr-deficient samples and temperature dependences of its emission intensity and decay times were studied in the detail. Room temperature decay time of about 180 ns and efficient and fast energy transfer from the host to the center of the 334 nm emission make this material promising candidate for X-ray phosphors.

1. Introduction

Ce-doped $SrHfO_3$ (SHO) is known phosphor material which is attractive due to high density (7.56 g/cm^3), low intrinsic radioactivity and fast response based on the Ce^{3+} 5d-4f emission [1]. It has been studied in recent years by several groups [2–6]. The Ce^{3+} doping at Sr^{2+} site induces coulombic disbalance in the lattice and the compensation mechanism has not been understood so far. The monovalent ion codoping was used to address this problem [5,6]. Apart from traditional solid state synthesis, the combustion synthesis [5,7] or sol–gel methods [4] have been used to prepare the powders. A few attempts were realized to prepare also optical ceramics [3,8] which indicate some practical potential of this material also in a bulk form.

Thermally induced ionization of the $5d_1$ excited state of Ce^{3+} in SHO has been reported recently [9], which shows the onset of this degrading process somewhat below room temperature (RT). The onset of this process shifts with increasing Ce concentration to higher temperatures when the 0.1% and 5%Ce samples were compared. Recently, the Pb^{2+} dopant has been proposed for SHO host [10,11]: such a phosphor shows even higher efficiency, emission in near UV around 340 nm and about one order longer photoluminescence decay time of about 200 ns with respect to the Ce^{3+} doped material. Very recently the systematic study of the excitation and emission characteristics in the undoped stoichiometric SHO has been performed [12] which reveals quite several UV–VIS emissions ascribed to the exciton and defect centers. In the Pb or Ce-doped SHO the competition between these "intrinsic" centers and the dopants was demonstrated. At RT the energy transfer to the dopants is dominant.

In this paper we continue our studies focused on the heavily Ce^{3+}-doped SHO. The processes of excited state ionization of Ce^{3+} center and concentration quenching are addressed as for their dependence on Ce concentration. New emission band at about 480 nm is found in heavily doped SHO:Ce and ascribed to the F^+ center. Furthermore, novel results achieved at the non-stoichiometric SHO are presented consisting of the excitation and emission spectra, temperature dependence (TD) of emission intensities, decay times and are completed further by the delayed recombination decay characteristics. New emission band at 334 nm is found in the Sr-deficient SHO and its origin is discussed.

2. Experimental

2.1. Sample preparation

For powder preparation the chemicals $SrCO_3$ (Johnson-Matthey Chemicals, grade 1), HfO_2 (Alfa Aesar, 99.95%) and CeO_2 (Koch-Light, 99.95%) were used. Powder samples were prepared by solid state reaction using a multiple step annealing procedures as follows (temperatures and duration in parenthesis are given): 500 °C (1 h) – 1100 °C (4 h) – 1170 °C (4–8 h). Two sets of samples were prepared, namely:

(1) $Sr_{0.99}Ce_{0.01}HfO_{3.01}$, $Sr_{0.95}Ce_{0.05}HfO_{3.05}$, $Sr_{0.9}Ce_{0.1}HfO_{3.1}$, $Sr_{0.85}Ce_{0.15}HfO_{3.15}$ (starting compositions) – these samples will be further denoted as Ce0.01, Ce0.05, Ce0.1 and Ce0.15, respectively,

* Corresponding author. Tel.: +420 220318445; fax: +420 233343184.
E-mail address: nikl@fzu.cz (M. Nikl).

0925-3467/$ - see front matter © 2011 Elsevier B.V. All rights reserved.
doi:10.1016/j.optmat.2011.04.040

(2) five samples of undoped SHO with starting compositions $Sr_iHf_{2-i}O_{4-i}$, $0.9 \leqslant i \leqslant 1.1$.

2.2. Experimental techniques

The XRD spectra were measured on the diffractometer Huber in arrangement with plane wave, the radiation was produced by the X-ray generator Rotaflex with rotating anode (Cu) of the firm Rigaku. The radioluminescence (RL), photoluminescence (PL) and photoluminescence excitation (PLE) spectra and PL decay kinetics were measured at temperatures within 77 (10)–500 K, using the custom made 5000 M Horiba Jobin Yvon fluorescence spectrometer. Oxford LN Optistat and Janis closed cycle cryostats were used to achieve the desired temperatures. The steady state spectra were excited by deuterium lamp (PL, PLE) and an X-ray tube (RL, Seifert). Measurement of fast PL decay was performed under excitation by the hydrogen-filled nanosecond coaxial flashlamp using the time-correlated single photon counting method. In the ms time scale the decays were measured under excitation by microsecond xenon flashlamp and using the multichannel scaling method. PLE spectra and decays in VUV–UV region were measured at Superlumi station, HASYLAB, DESY, Hamburg [13]. All the spectra were corrected for the spectral dependence of the apparatus characteristics. True decay times were obtained using the convolution of the instrumental response function with an exponential function(s) and the least-square-sum-based fitting program (SpectraSolve software package, Ametec). Errors of calculated decay time values are typically few percent.

3. Results and discussion

3.1. Structural characterization

XRD spectra were measured for each sample. In the case of all heavily Ce-doped samples, XRD spectra showed minor content of CeO_2 and HfO_2 compounds. In the case of Ce0.15 sample, Fig. 1, three phases, namely, the orthorhombic SHO (ICDD Card No. 88-14), monoclinic HfO_2 (ICDD Card No. 34-104) and cubic CeO_2 (ICDD Card No. 34-394) were found. Phase analysis found for their contents (in wt%) the ratio 90:4:6, respectively.

In case of nonstoichiometric samples the XRD spectra show very minor content of HfO_2 and SrO for the Sr-deficient and Sr-rich samples, respectively. The detailed XRD spectra analysis of these samples will be reported elsewhere.

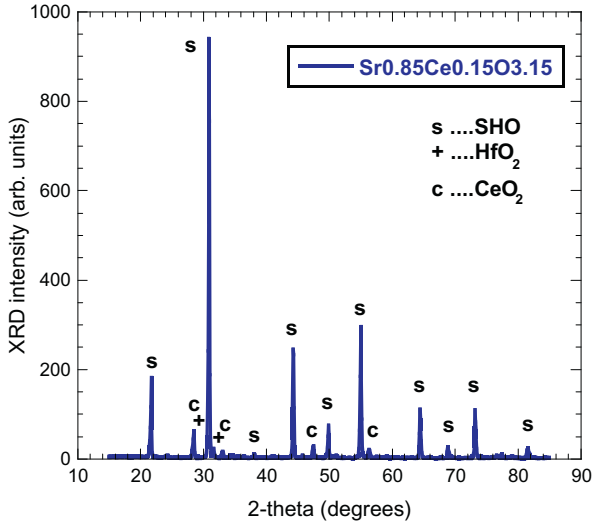

Fig. 1. XRD spectrum of the Ce0.15 sample.

3.2. Heavily Ce-doped $SrHfO_3$

Radioluminescence spectra of the set of SHO:Ce samples are in Fig. 2. The Ce^{3+} emission at 410 nm [2–9] is accompanied by the band at about 335 nm and clear competition between these two bands is noted. Ce^{3+} emission intensity increases up to Ce0.1 sample. The origin of the 335 nm band is in question as it has not been observed in the stoichiometric undoped SHO [12]. Its spectral position is very close to that of Pb^{2+} center [10,11], but contamination by Pb ions is practically excluded in these samples (checked by ICP analysis). It is most probably related to the Sr-deficient SHO phase which is also supported by the residual content of HfO_2 compound in both the Ce-doped and Sr-deficient samples, see further in Section 3.2.

It has been noted in [9] that higher Ce concentration is beneficial for the shift of the onset of $5d_1$ state thermally induced ionization towards higher temperatures. Due to this observation a careful analysis of PL decays measured at RT was made, Fig. 3, for all the samples from Fig. 2. In fact, in all the samples but Ce0.01 the decay must be approximated by the sum of two exponential terms $I(t) = A1\exp[-t/T1] + A2\exp[-t/T2] + \text{background}$. While the exponential tail of the decay curve characterized by the longer decay

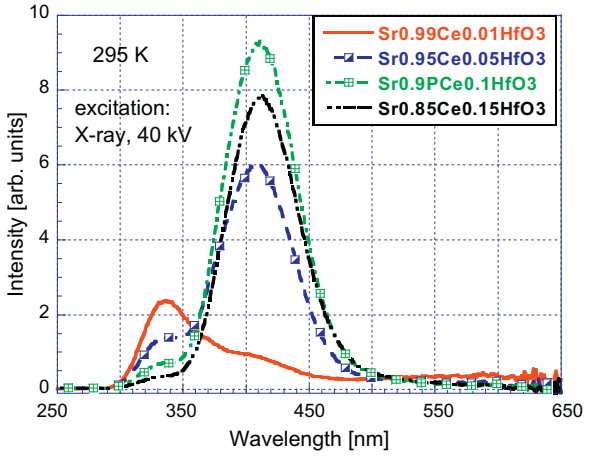

Fig. 2. Radioluminescence spectra of Ce-doped SHO (starting composition noted in the legend). Excitation by X-ray, 40 kV.

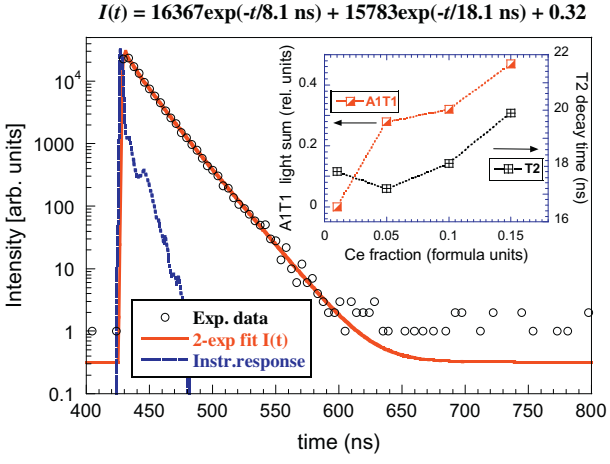

Fig. 3. PL decay for Ce0.1 sample, exc = 310 nm, em = 400 nm. Decay is approximated by 2-exponential function $I(t)$ given in the figure. In the inset the evaluation of relative lightsum of faster component $A1T1/(A1T1 + A2T2)$ and the value of $T2$ decay time are given depending on the Ce fraction, see also the text.

time $T2$ is defined by the transition characteristics of the Ce^{3+} center itself, the distortion (acceleration) of the initial part of the decay points to an energy transfer or concentration quenching process. Due to heavy Ce doping the latter process can be a logical consequence. The relative weight (lightsum) of the faster component is calculated as $I_1 = A1T1/(A1T1 + A2T2)$ and can be used to evaluate quantitatively the distortion of the decay from a single exponential course, i.e. the intensity of concentration quenching effect. Such an evaluation was performed and the dependence of I_1 and $T2$ on Ce concentration is shown in the inset of Fig. 3. In fact, one can see clearly increasing relative value of the I_1 with Ce concentration which points to increasing concentration quenching effect. It appears, however, relatively mild up to the Ce0.1 sample at least. The value of $T2$ is increasing with Ce concentration as well, which indicates the shift of the knee of thermally induced ionization of $5d_1$ state of Ce^{3+} center towards higher temperatures [9]. The two effects described will have the opposite influence on the scintillation efficiency of Ce^{3+}-doped SHO. Consequently, an optimum Ce concentration must exist which seems to be close to that in Ce0.1 sample. It is consistent with the observed RL intensity dependence in Fig. 2. The decay time of the 335 nm band is of about 170 ns in all the samples.

TD of PL spectra of Ce0.05 sample has been already published under the direct excitation into 4f-$5d_1$ absorption band of Ce^{3+} at 310 nm [9]. Flat dependence on the temperature was obtained until some 230 K with gradual decrease up to RT and steeper decrease at higher temperatures. Such measurement can be influenced by temperature dependent absorption coefficient of Ce^{3+} 4f-$5d_1$ absorption band due to light collection from rather thin sample layer because of light scattering in the powder. Therefore, the same measurement was performed under band-to-band excitation at 200 nm, Fig. 4. However, rather different spectral pattern was obtained at the lowest temperatures, in which the spectrum is dominated by a broad band peaking at about 450 nm and the Ce^{3+} emission at 410 nm appearing just like a shoulder, Fig. 4a. The former emission is completely quenched at about 200 K, while the Ce-related one increases up to approx. 350 K and becomes weaker again at higher temperatures. The integral of PL spectrum above 200 K is displayed together with the mentioned TD from Ref. [9] and clearly different behavior of the Ce^{3+} emission intensity is noted for both excitation wavelengths. Though the TD course at 200 nm excitation can be influenced by an energy transfer host $\Rightarrow Ce^{3+}$, the emission intensity decrease above 300 K is definitely less pronounced with respect to the other TD measured under the 310 nm excitation. As the penetration depth in the case of 200 nm excitation is much smaller (absorption coefficient in the exciton absorption region will be several orders higher respect to that in 4f-$5d_1$ absorption band of Ce^{3+}) and is estimated of the order of 1 μm the mentioned above effect of temperature dependence of the 4f-$5d_1$ absorption coefficient could be indeed important. In other words, the true TD of the 410 nm emission of Ce^{3+} will be above 300 K between two curves in Fig. 3.

To complete luminescence characteristics of the 450 nm emission band, its excitation spectrum and decay were measured at 77 K in Figs. 5 and 6, respectively. PLE spectrum shows three bands at about 410–420 nm, 270–280 nm and 220–230 nm and efficient excitation in the SHO band edge as well. The decay is dominated by fast component of about 6–7 ns decay time and somewhat slower possibly non-exponential tail is present as well. Small Stokes shift of a few tenths of eV, broad emission band and fast ns decay are typical for the F^+ centers in complex oxides, e.g. in $Y_3Al_5O_{12}$ [14], $YAlO_3$ [15,16]. $Lu_3Al_5O_{12}$ [17] and $Lu_4Hf_3O_{12}$ [18] so that we ascribe the 450 nm emission to the F^+ center in SHO as well.

The mechanism of the Ce^{3+} incorporation into SHO host in such high concentrations is worth to be discussed. According to the phase analysis, in the sample Ce0.15 there remains certain amount of CeO_2 (6 wt%) and of HfO_2 (4 wt%) separated from the SHO phase.

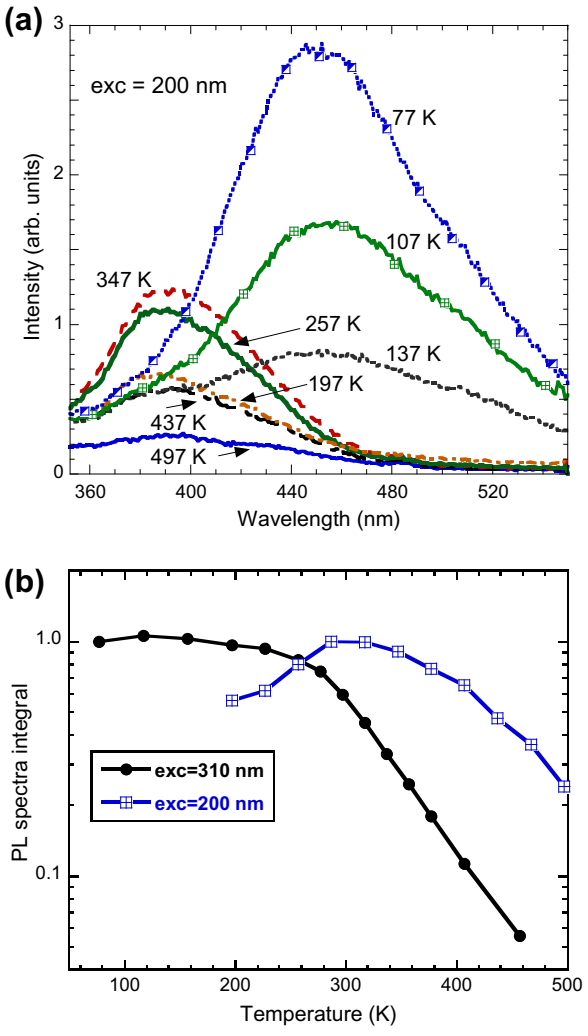

Fig. 4. Temperature dependence of (a) PL spectra of Ce0.05 sample. Excitation at 200 nm, (b) integral of PL spectra for exc = 310 nm and 200 nm (in the latter for the temperatures above 200 K only).

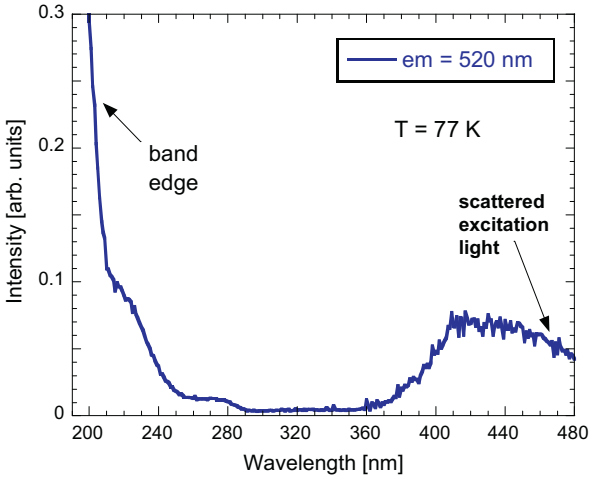

Fig. 5. PLE spectrum of the 450 nm band at 77 K. Emission wavelength at 520 nm was chosen to reduce the effect of scattered light in the measurement of a powder sample, which does distort the measurement above approx. 440 nm.

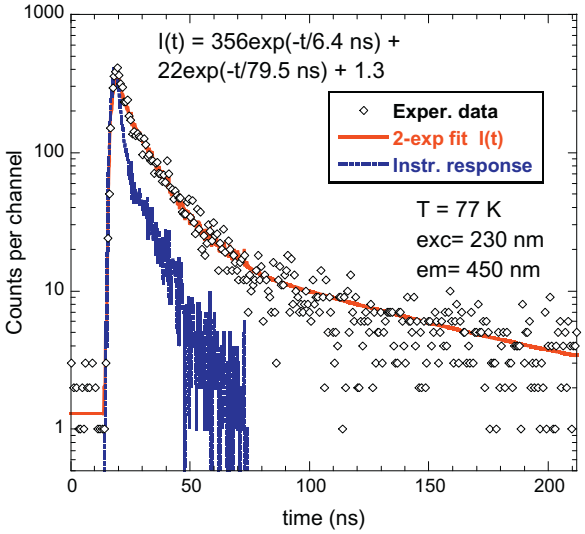

Fig. 6. PL decay of the 450 nm band under excitation in the higher 220–230 nm excitation band close to the band-edge of SHO. $T = 77$ K. Solid line is convolution of function $I(t)$ with the instrumental response.

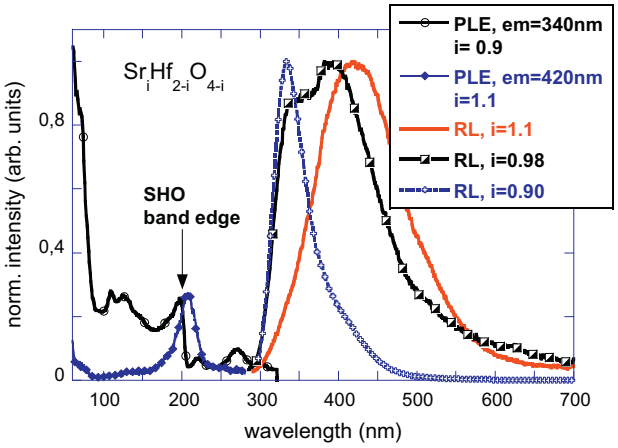

Fig. 7. PLE and RL (excitation by X-ray, 40 kV) spectra of undoped SHO powders with varying stoichiometry.

When we compare these data with the starting composition of the sample, we can determine what amount of the starting components was incorporated in the SHO phase, and then to determine the SHO phase composition, which results in the formula F1: $Sr_{0.935}Ce_{0.035}Hf_{1.030}O_{3.047}$.

Cerium can enter the SHO phase as Ce^{3+} and also as Ce^{4+}, in both cases the formula F1 is practically the same. The Ce^{3+} ion enters very probably the strontium site, for its occurrence in positions of hafnium we do not find any support in our experiments. The distinct surplus of hafnium in the SHO phase supports also the hypothesis that all cerium in the SHO phase in the sample Ce0.15 is embedded in the strontium sites as Ce^{3+}. Owing to a great chemical dissimilarity of both the main components we also assume that the Hf^{4+} ions do not enter the positions of Sr^{2+}, and vice versa. It follows then from the difference between the indexes in the formula F1 $(1.030 - (0.935 + 0.035) = 0.06)$ that 6% of Sr-positions in the phase SHO of the sample Ce0.15 is vacant. Concentration of the charge balancing oxygen vacancies is not 6%, but only 4.25%, as part of oxygen sites (1.75%) is occupied by oxygen bound to the Ce^{3+} ions. Presence of the oxygen vacancies in the SHO phase is supported by the presence of the F^+ centers in the SHO:Ce samples. The strontium vacancies play a role in the 334 nm luminescence band formation which is visible in Fig. 2, and will be described in the details in Section 3.3 below which deals with the Sr-deficient SHO.

3.3. Nonstoichiometric SHO

To complete further the luminescence characteristics and study possible influence of SHO stoichiometry, the set of several samples of varying stoichiometry, $Sr_iHf_{2-i}O_{4-i}$, $0.9 \leqslant i \leqslant 1.1$ was prepared and characterized. PLE and RL spectra are in Fig. 7. The Sr-rich sample shows the 420 nm band which has been already reported in the stoichiometric SHO sample prepared by sol–gel method [12]. Its PLE spectrum shows the maximum around 210 nm just below the band-edge which is consistent with the trapped exciton and/or defect origin proposed in Ref. [12]. Very low excitation efficiency is noted above the gap within approx. 90–170 nm. Below 90 nm the onset of electronic multiplication is evident. In the opposite nonstoichiometric limit, the Sr-deficient sample shows strikingly different luminescence spectrum dominated by the 334 nm band which is practically identical with that observed in Fig. 2. This emission is very efficiently excited in the band edge and above it as well, which points to efficient energy transfer to this center from SHO host. Another two excitation bands at about 221 nm and 270 nm, i.e. below the band-gap, point to the defect-origin of the 334 nm band.

TD of the 334 nm emission was measured within 77–500 K (see examples of spectra in the inset of Fig. 8) and the spectra were integrated to evaluate their temperature dependence, Fig. 8. Mild increase or temperature independent course is noted up to 320 K followed by the double-slope decrease where the steeper slope starts around 400 K.

PL decays of the 334 nm emission were measured under the excitation at 270 nm and decay times evaluated in the 10–500 K temperature interval, Fig. 9. Excellent single exponential decays were obtained through 2–3 orders of magnitude up to 400 K at least. Low temperature limit of PL decay time is 286 μs ($T = 10$ K) with the knee on the TD at about 50 K. Single slope of TD of decay times extends then up to 400 K followed by the steeper decrease of decay time values, see inset of Fig. 9. To get information about the speed of energy transfer from the host the decay of 334 nm band was measured in DESY under 270 nm and 110 nm excitations,

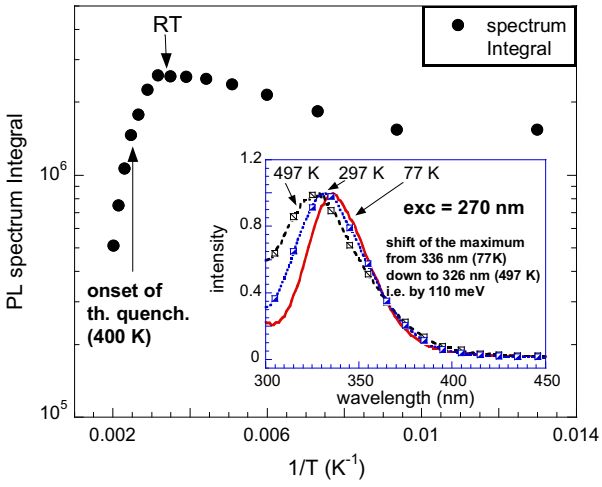

Fig. 8. Temperature dependence of the 334 nm emission band (PL spectra integrals), exc = 270 nm. In the inset the examples of the PL spectra at 77, 297 and 497 K are given which show approx. 110 meV high energy shift of the band within 77–497 K.

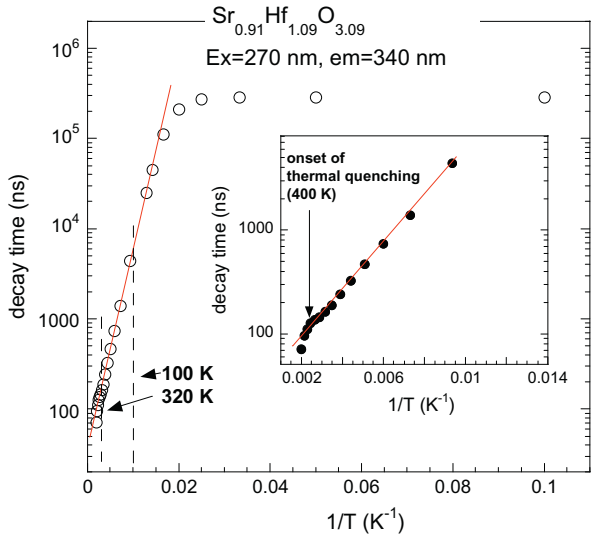

Fig. 9. PL decay time temperature dependence related to the 334 nm band under excitation in the lowest absorption/excitation band at 270 nm. Solid line is just to guide the eye.

Fig. 10. In the latter case only small build-up and slowing-down of the decay was obtained (decay time increased from 176 ns to 189 ns) and the relative signal level before the rising edge of the decay respect to decay amplitude is comparable for both excitations which means that under 110 nm excitation there is no considerably slower decay component underlying the measured decay curve in the 200 ns time window.

The obtained TD's of emission intensity and decay time of the 334 nm band point to the two-excited-level scheme (so called three level model) frequently applied to model the TD of self-trapped exciton emission intensity and decay times in other complex oxides [19–21]. The onset of thermal quenching is indicated at about 400 K. Gradual increase of emission intensity within 100–200 K in Fig. 8 is not clear and needs further study. It could be caused e.g. by temperature dependence of the 270 nm absorption band or by other temperature dependent non-relaxed excited state characteristics.

To get more insight in the processes occurring in the excited state of the 334 nm emission we employed the measurement of

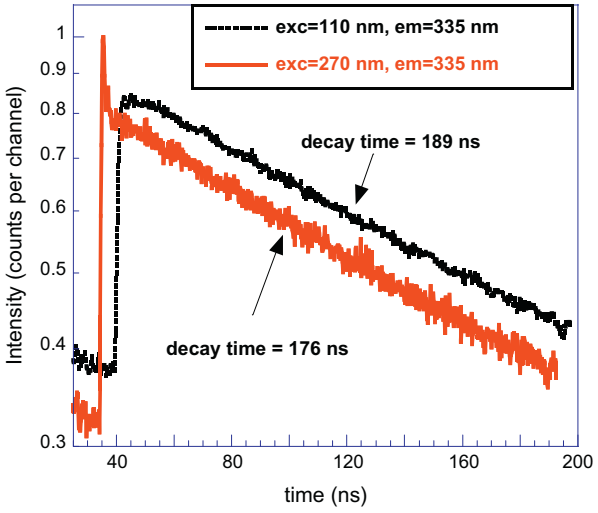

Fig. 10. PL decay of the 334 nm emission band at RT in $Sr_{0.91}Hf_{1.09}O_{3.09}$, under excitation at 270 nm and 110 nm, measured at Superlumi station, DESY. Decays are horizontally and vertically shifted for clarity.

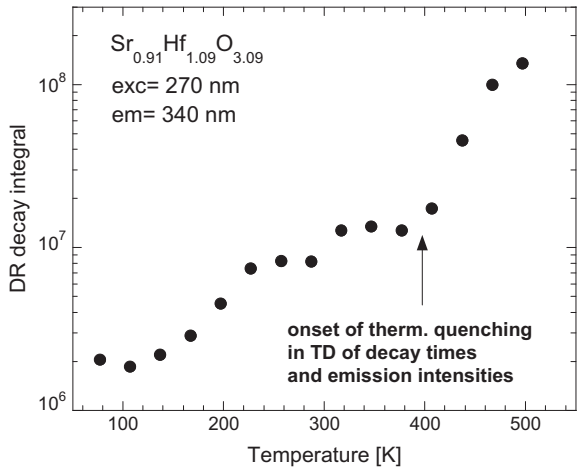

Fig. 11. Temperature dependence of the delayed recombination decay integral of the 334 nm emission band under excitation in the lowest energy absorption band of the center at 270 nm.

the delayed recombination decay of this emission similarly as done in the Pr-doped LSO and YSO [22] or Ce-doped SHO [9] as well. The decay is measured at the same excitation/emission wavelengths, but in an extended ms time scale to monitor any delayed recombination processes arising due to the escape of electron from the excited state of luminescence center to the conduction band or any trap nearby and its return and radiative recombination at the center at later times. This technique proved very successful to detect thermally induced ionization of the luminescence center excited state and due to its purely optical character it can be applied also to powders as shown e.g. for LPS:Pr [23]. Temperature dependence of the delayed recombination decay integrals (first point which contains the prompt ms component is omitted in the integration) is given in Fig. 11. There is no immediate explanation of the step-like increase of the integral value within 120–320 K, but the nanosecond decay time values in Fig. 9 are of perfectly "single-slope" dependence within this temperature interval which excludes any additional effects occurring in the relaxed excited state of the center. Steep increase of the integral above 400 K is correlated with the onset of thermal quenching evidenced in TD of decay times and emission intensities in Figs. 8 and 9. Thus, the thermal ionization of the center is identified as one possible cause of the 334 nm band quenching.

It seems difficult to propose the nature of the emission center responsible for the 334 nm emission band basing on the present experimental data. As it is related to a defect and it is arising in a Sr-deficient SHO structure, the Sr vacancy should play a role in such a luminescent center creation. Great similarity is found with the exciton luminescence in tungstates or molybdates where the luminescence process occurs as a charge transfer transition in the oxyanion group with possible participation of heavy divalent cation in the absorption transition, i.e. non-relaxed excited state of the center, in case of $PbWO_4$ see e.g. [24,25]. The relaxed excited state of the luminescence center in these materials (d-orbital of Mo^{6+} or W^{6+} ions) might be analogous to that in SHO [26,27]. However, further research is needed to provide a well-grounded hypothesis for the nature of the 334 nm emission center in Sr-deficient SHO.

4. Conclusions

Heavily Ce-doped $SrHfO_3$ phosphors and and the undoped non-stoichiometric ones were prepared by solid state reaction and characterized by several luminescence methods. In case of the Ce-doped

samples the highest radioluminescence intensity is obtained for $Sr_{0.9}Ce_{0.1}HfO_{3+0.1}$ composition. In PL decay the effect of concentration quenching and of the position of the onset of $5d_1$ excited state ionization was demonstrated and discussed. New emission band at 450 nm was revealed with decay time of about 6–7 ns at 77 K and ascribed to the F^+ center.

Stoichiometry of $SrHfO_3$ appears to have a crucial impact on its luminescence properties. The Sr-rich sample shows the dominant emission at 420 nm, the RT excitation of which is most efficient just below the band edge at about 210 nm and efficiency of excitation above the gap within 90–170 nm is very low. The Sr-deficient $SrHfO_3$ shows new emission band at 334 nm, which is excited both below the gap at 270 and 220 nm and very efficiently also in the band edge and above the gap. Room temperature PL decays excited at 270 nm and 110 nm show very similar decay times of 176 ns and 189 ns, respectively, and no underlying slower component is noted in the latter case. It points to an efficient and fast energy transfer from the host to the center of the 334 nm emission. Temperature dependences of emission intensity and decay times of the 334 nm band can be explained by the two-excited-state level arrangement similar to that of the exciton luminescence in tungstates and molybdates. The onset of thermal quenching is found well above RT at about 400 K. Thermally induced ionization of the relaxed excited state of the emission center is found above this temperature as well and can be one of the reasons of the quenching process.

Acknowledgements

Financial support of GAAV KAN 300100802 and GACR 202/08/0893 projects is gratefully acknowledged together with the joint project of AS CR-CNR (2010–2012) and DESY HASYLAB project II-20100033. J. Drahokoupil is acknowledged for the phase analysis of the XRD spectra.

References

[1] S.L. Dole, V. Venkataramani, Alkaline-earth hafnate phosphors with cerium luminescence, US. Patent #5124072, 1992.
[2] H. Retot, A. Bessiere, A. Kahn-Harari, B. Viana, Opt. Mater. 30 (2008) 1109.
[3] E.V. Van Loef, W.M. Higgins, J. Glodo, Ch. Brecher, A. Lempicki, V. Venkataramani, W.W. Moses, S.E. Derenzo, K.S. Shah, IEEE Trans. Nucl. Sci. 54 (2007) 741.
[4] M. Villanueva-Ibanez, C. Le Luyer, S. Parola, O. Marty, J. Mugnier, J. Sol–Gel Sci. Technol. 31 (2004) 277.
[5] Y.M. Ji, D.Y. Jiang, L.S. Qin, J.J. Chen, T. Feng, Y.K. Liao, Y.P. Xu, J.L. Shi, J. Cryst. Growth 280 (2005) 93.
[6] S.M. Loureiro, Y. Gao, V. Venkataramani, J. Am. Ceram. Soc. 88 (2005) 219.
[7] A. Lauria, N. Chiodini, E. Mihokova, F. Moretti, A. Nale, M. Nikl, A. Vedda, Opt. Mater. 32 (2010) 1356.
[8] E.V. van Loef, Y. Wang, S.R. Miller, C. Brecher, W.H. Rhodes, G. Baldoni, S. Topping, H. Lingertat, V.K. Sarin, K.S. Shah, Opt. Mater. 33 (2010) 84.
[9] V. Jary, E. Mihokova, M. Nikl, P. Bohacek, A. Lauria, A. Vedda, Opt. Mater. 33 (2010) 149.
[10] E. Mihokova, F. Moretti, N. Chiodini, A. Lauria, M. Fasoli, A. Vedda, A. Nale, M. Nikl, P. Boháček, IEEE Trans. Nucl. Sci. 57 (2010) 1245.
[11] V. Jary, M. Nikl, E. Mihokova, P. Bohacek, B. Trunda, K. Polak, V. Studnicka, V. Mucka, Radiat. Measure 45 (2010) 406.
[12] E. Mihóková, N. Chiodini, M. Fasoli, A. Lauria, F. Moretti, M. Nikl, V. Jarý, A. Vedda, Phys. Rev. B 82 (2010) 165115.
[13] G. Zimmerer, Radiat. Measure 42 (2007) 859.
[14] M. Springis, A. Pujats, J. Valbis, J. Phys. Cond. Mater. 3 (1991) 5457.
[15] L. Grigorjeva, A. Krasnikov, V.V. Laguta, M. Nikl, S. Zazubovich, J. Appl. Phys. 108 (2010) 053509.
[16] Yu. Zorenko, A.S. Voloshinovskii, I.V. Konstankevych, Opt. Spectr. 96 (2004) 532.
[17] V. Babin, V.V. Laguta, A. Maaroos, A. Makhov, M. Nikl, S. Zazubovich, Phys. Stat. Sol. (b) 248 (2011) 239.
[18] E. Mihóková, M. Fasoli, A. Lauria, F. Moretti, M. Nikl, V. Jary, R. Kucerkova, A. Vedda, Prompt and delayed recombination mechanisms in $Lu_4Hf_3O_{12}$ nanophosphors, Opt. Mater., submitted for publication.
[19] G. Blasse, G. Bokkers, J. Solid State Chem. 49 (1983) 126.
[20] M. Itoh, T. Kajitani, Phys. Stat. Sol. (b) 248 (2011) 422.
[21] M. Nikl, P. Bohacek, E. Mihokova, M. Kobayashi, M. Ishii, Y. Usuki, V. Babin, A. Stolovich, S. Zazubovich, M. Bacci, J. Lumin. 87–89 (2000) 1136.
[22] J. Pejchal, M. Nikl, E. Mihokova, A. Novoselov, A. Yoshikawa, R.T. Williams, J. Lumin. 129 (2009) 1857.
[23] M. Nikl, A.M. Begnamini, V. Jary, D. Niznansky, E. Mihokova, Phys. Stat. Sol. RRL 3 (2009) 293.
[24] V. Murk, M. Nikl, E. Mihokova, K. Nitsch, J. Phys. Cond. Mat. 9 (1997) 249.
[25] Y.B. Abraham, N.A.W. Holzwarth, R.T. Williams, G.E. Matthews, A.R. Tackett, Phys. Rev. B 64 (2001) 245109.
[26] Z. Feng, H. Hu, S. Cui, C. Bai, H. Li, J. Phys. Chem. Solids 70 (2009) 412.
[27] D. Cherrad, D. Maouche, Physica B 405 (2010) 3862.